Geometrical and Structural Analysis in the High Folded Zone between Harir and Bradost Anticlines, Northeast Iraq Using Geoinformatics Techniques

Ahmed T. Shihab **Mustafa R. Al-Obaidi**
Department of Geology, College of Science, University of Baghdad
ahdsat1975@gmail.com mustafa.r.s.alubaidi@gmail.com

Abstract

The arrangement of fold types and thrust system within the study area was analyzed using satellite image, GIS and field work. Attitudes of the bedding planes were extracted through eleven QuickBird scenes using the Structural Contour Lines (SCL) method. These results have been compared with dip angles and dip directions, which measured in the field. Building of SCL based on high spatial resolution of QuickBird images, and Digital Elevation Models (DEMs) is a key role to understand the geometrical properties of the anticlines in this study. The aim of this paper is to determine the geometric and the structural deformation analysis by using geoinformatics techniques and to update the geological and structural map of the High Folded Zone of the Zagros-Taurus orogenic belt, northeast part of Iraq. We generate DEMs from stereo image of the Advanced Spaceborne Thermal Emission and Reflection Radiometer (ASTER) along-track sensors. We simulated the geometry of one anticline based on the 3D representation modeled. According to the structural contour map, the faults within this area formed sequentially as the deformation front migrated from the collision zone towards the NE. Movement up thrust ramps created fault-bend folds behind which serial detachment folding developed in the cover.

Keywords: Digital Elevation Models (DEMs); attitudes extraction; structural deformations; Advanced Spaceborne Thermal Emission and Reflection Radiometer (ASTER); remote sensing; GIS; Zagros – Taurus

الخلاصة

تم تحليل أنظمة ترتيب انواع الطيات والفوالق العكسية ضمن منطقة الدراسه بأستخدام الصور الفضائية، نظم المعلومات الجغرافية والعمل الحقلي. تم استخراج ميل ومضرب الطبقات بأستخدام طريقة الخطوط الكنتوريه التركيبية وذلك بالأعتماد على احد عشر مشهد للقمر الصناعي QuickBird وتم مقارنة هذه النتائج مع القياسات الحقلية. ان عملية بناء الخطوط الكنتوريه التركيبية من خلال الأعتماد على بيانات او مشاهد للقمر الصناعي QuickBird ذات الدقه العالية بالأضافه الى موديل قيم الأرتفاعات الرقمية (DEMs) كان لها الدور الرئيسي في فهم خصائص او مواصفات التركيب الهندسي للطيات المحدبة الموجودة في منطقة الدراسة. ان هدف هذه الدراسة هو تحديد الأشكال التركيبية الهندسية بأستخدام تقنيات التحسس النائي ونظم المعلومات الجغرافية (geoinformatics techniques) في نطاق الطيات العالية والمتأثرة بالحركات البانيه للجبال لزاكروس وطورس، شمال شرق العراق وتحديث الخريطة التركيبة والجيولوجية لمنطقة الدراسة بالأعتماد على العمل الحقلي و التفسير البصري للصور الفضائية. تم أستخراج قيم الأرتفاعات الرقمية من بيانات القمر الصناعي (ASTER) بالأعتماد على تقنية تجسيم الصور على طول المسار لمشهد هذا القمر او المتحسس (along-track sensors). ثم تم بعد ذلك عمل محاكاة الشكل الهندسي لأحدى الطيات بالأعتماد على التمثيل الثلاثي الأبعاد. اظهرت الخارطة التركيبية أن الفوالق التي تقع ضمن هذه المنطقة تشكلت وبشكل متعاقب نتيجة حركة النقل للتشوهات في منطقة التصادم باتجاه الشمال الشرقي. ان الحركة الى الأعلى على سطح المنصة المائل (ramp) في الفوالق العكسية كونت نظام من الفوالق المصاحبه للطيات (fault-bend folds) وانتجت ايظا سسلسلة من الطيات من نوع الطيات الانزلاقية (detachment folding) في الغلاف الصخري.

الكلمات الدالة: موديل الأرتفاع الرقمي، استخراج الميل والمضرب، الأشكال التركيبية، المتحسس استر، التحسس النائي، نظم المعلومات الجغرافية، زاكروس – طوروس.

1.Introduction

Geometrical characteristics of the anticlines are commonly adapted from field measurement data. These measurements can be made at the localities of accessible areas. Inaccessible areas, consider handicap to measure the attitude of strata (i.e., strike and dip). It made the reasons that may not give a good geometrical property of structural form. The study area characterizes by complex geological structures and some areas along the flanks of the anticlines are difficult access.

In the recent years, Remote Sensing (RS) and Geographic Information System (GIS) are widely used in different geological sciences particularly in the structural geology due to the fruitful results provided by their analysis. Despite, the evolution in the techniques of RS and GIS, but the study of structural geology using these techniques is still weak or insufficient. The use of RS data increases the efficiency of field mapping, especially in the complex and poorly accessible terrain areas where the fieldwork can be challenging, time-consuming and costly.

Stereo image of the ASTER along-track sensors is still the most common method used for generating DEMs. Many articles such as (Lang *et al.*, 1996; Toutin and Cheng, 2001; Kääb *et al.*, 2002; Büyüksalih *et al.*, 2003; Hirano *et al.*, 2003; Eckert *et al.*, 2005; Poli *et al.*, 2005; Watanabe, 2006; Oliveira and Paradella, 2008; Toutin, 2008; Zhao *et al.*, 2011; Cuartero *et al.*, 2012) addressed the subject of DEMs generated from ASTER stereoscopic images and its accuracy. Attitudes extraction using map pattern or the three-point problem methods have been explained in many textbooks e.g. (Bennison, 1990; Allison, 2004; WVDEP, 2005; Ragan, 2009).

Reif *et al.*, (2011) studied the quantitative structural analysis in Kurdistan, northeast Iraq. They presented a newly developed software tool for interactively mapping and measuring the spatial orientation (i.e., dip angle and dip direction) using remote sensing techniques and structural field data. Dadon *et al.*, (2011) studied the ability of extracting structural information from a spaceborne imaging using GIS. They presented a semi-automated GIS model for extracting structural information of sedimentary rocks by combining the imaging spectrometry classification with a digital terrain model. The output consists of a database with structural attributes, specifically the dip and strike, of the geological layers.

Hasbargen, (2012) highlighted the effects of three-point method and developed mathematical formula to calculate the dip angle using a wide variety of freely available online remotely sensed data of the (DEMs). He was pointed out to that the confidence measurements done by a geologist in the field with a compass and inclinometer are “ground truth,” but there are limitations to field investigations. Where, a surface that is measured by hand is typically on the order of a few square centimeters in dimension, and thus may not be truly representative of the orientation over a longer length of 10s to 100s m. In addition, poorly defined bedding surfaces can make it difficult to find a suitable plan to characterize strike and dip angles.

Satellite images with spatial resolutions down to tens of centimeters in some cases can be used to interpret both ductile structures, such as folds, and brittle faults and fractures are mappable from satellite images and aerial photos (Fossen, 2010). These measurements and interpreted information with the data obtained from field measurements and investigation can be enhanced the results of structural analysis. Satellite images are now available at increasingly high resolutions and are a valuable tool for the mapping of map-scale structures, and may be combined with digital elevation data to create three-dimensional model (Fossen, 2010).

The objective of this study is to characterize the geometrical properties of some structural elements, and to produce digital structural map using both, field and remotely sensed data. This study included three main steps: (1) Extracting DEMs having spatial resolution of 15m from ASTER stereo image; (2) Computing attitudes of bedding plane and structural contour line depends on overlying topographical contour line derived from DEMs and QuickBird images; and (3) Updating the geological map of the study area and delineating some structural elements (i.e., structural map) based on photo-interpretation and field investigations.

2.Study Area

The study area is located in the northern part of Iraq. It is laid within the HFZ, which is a part of the unstable shelf of Arabian Plate. It covers an area around 1086km²; lying between the following geographical coordinates: 36° 30′- 36° 53′ 45′′ N Latitudes; 44° 00′ - 44° 30 E Longitudes (Figure. 1).

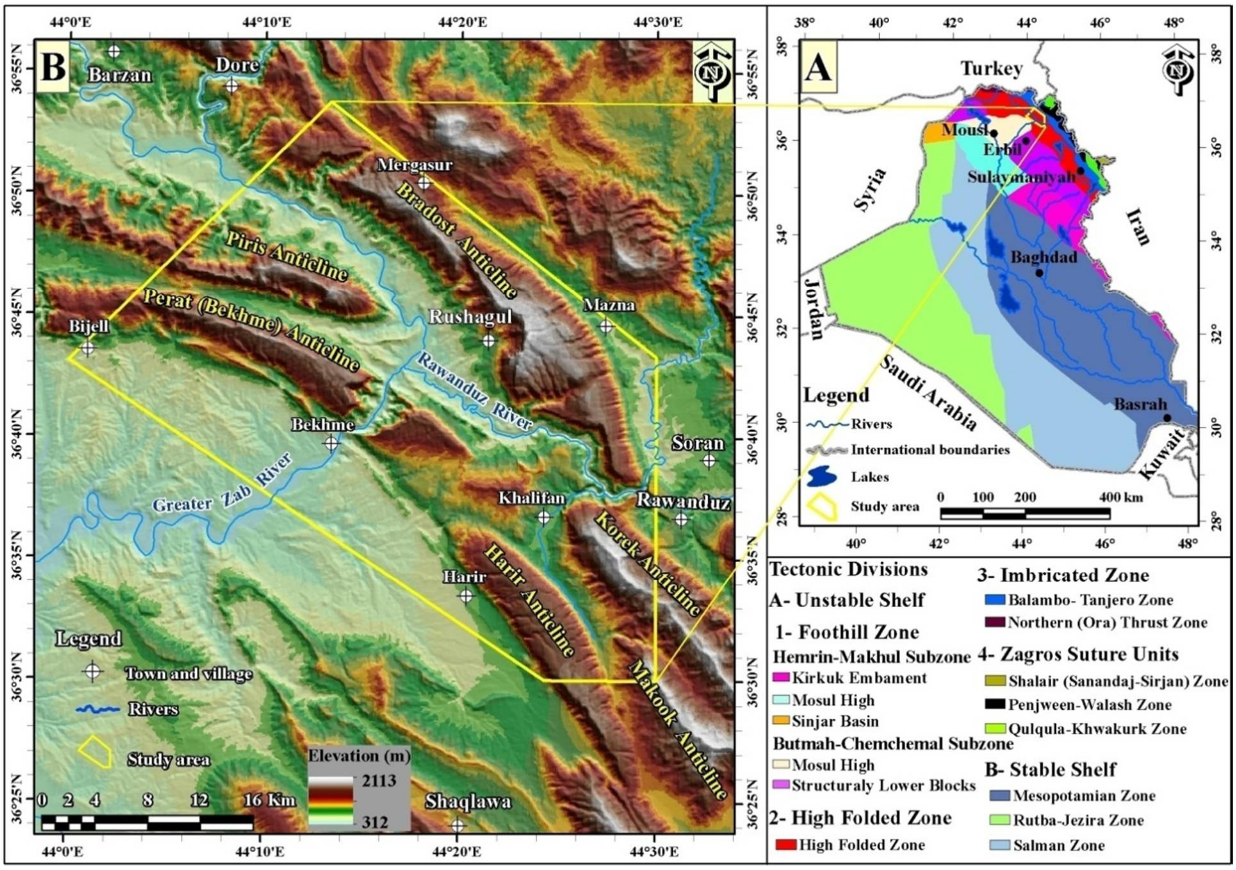

Figure 1. Location map of the study area in the HFZ (A): tectonic zones of Iraq after (Jassim and Goff, 2006). (B): color coded of DEMs adopted from Shuttle Radar Topography Mission (SRTM).

It is one of the relatively complex geological structures within the foreland folds belts or the Zagros Fold-Thrust Belt (ZFTB) of the Zagros orogenic belt, which is a part of the Alpine–Himalayan mountain chain (Alavi, 1994). It includes five anticlines, these are: Bradost, Piris, Perat (Bekhme), Harir, and Korek.

2.1. Geological Setting

Both E-W Taurus and NW-SE Zagros trending in the north and northeastern of Iraq was formed by the closure of the Neotethys and the continental collision of the Arabian Plate with the Turkish and Iranian Plates (Jassim and Goff, 2006). The study area takes a possession of changing in trending of the fold axes. These axes tend to be E-W trending in the north and northwestern part of the study area, while in the southern and southeastern part till the Greater Zab River it becomes corresponding with the NW-SE trending (Sissakian, 2012) see Figure (1). The HFZ forming an arch shaped belt with different widths. It runs from the Turkish border in the NW Iraq to the Iranian border, in the SE (Al-Kadhimi *et al.*, 1996).

The geological formations of the study area can be described depending on the structural forms; the majority of anticlines are built up by Cretaceous rocks. Moreover, in the core of many anticlines, Jurassic rocks are exposed. Whereas, the synclines are formed by Upper Cretaceous and rarely Paleogene rocks (Figure 2), which depending on both field observation and the previous works of (Ibrahim *et al.*, 1984; Sisakian, 1998; Omar, 2005) the exposed formations are explained briefly in table (1):

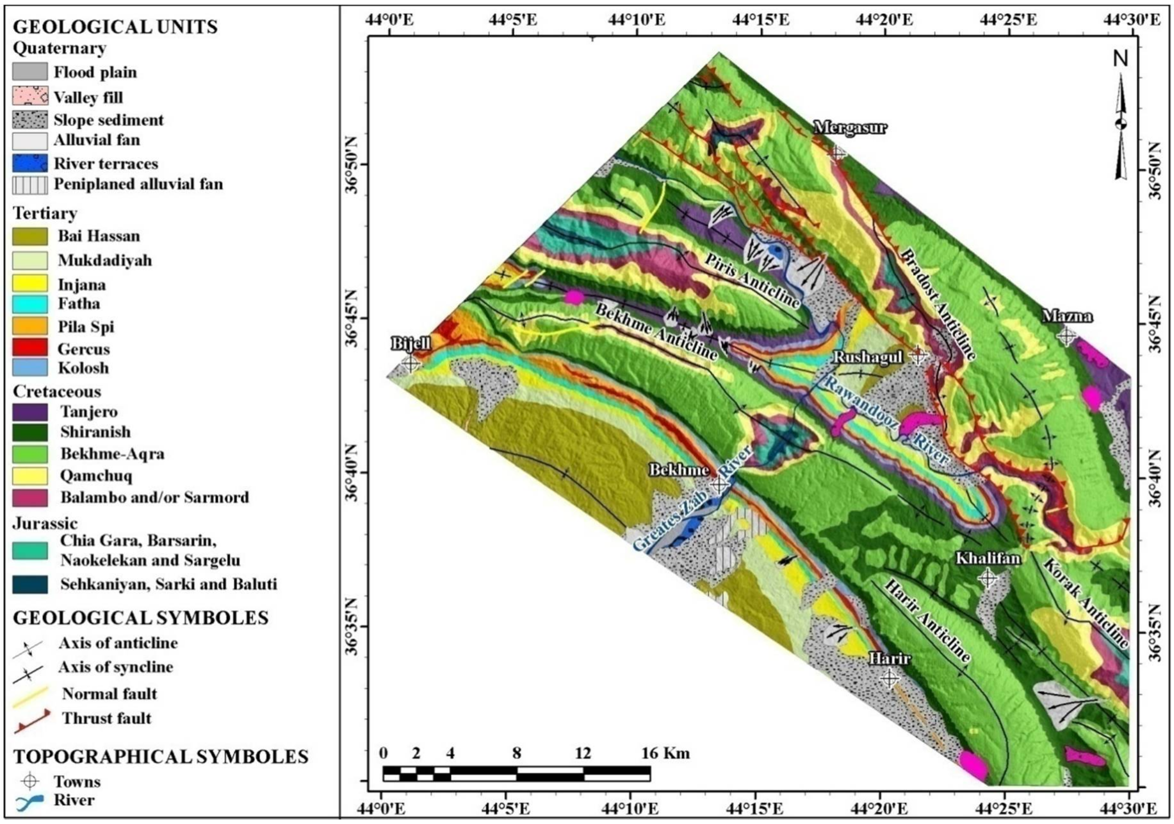

Figure 2.Geological map of the study area after (Ibrahim *et al.*, 1984; Sisakian, 1998).

Table 1: General lithology of the stratigraphic units in the study area

Geologic age		Stratigraphic units	Lithology
Tertiary		Bai Hassan	Alteration conglomerate, sandstone and clystone
		Mukdadiyah	Cycle deposits of pebbly sandstone, siltstone and clystone
	Miocene	Injana	Cycle deposits of red sandstone, siltstone and clystone
		Fatha	Thick red claystone, siltstone, limestone, marl, and gypsum
	Eocene	Pila Spi*	Mainly well bedded limestone
		Gercus	Red sandstone, siltstone and clystone
	Palaeocene	Kolosh	Black claystone, siltstone and sandstone
Cretaceous	Late	Tanjero	Khaki sandstone, claystone with conglomerate intermingling with olive green marl
		Shiranish	Well bedded limestone and blue marl
		Bekhme-Aqra*	Well bedded very hard dolomitic limestone
	Early	Qamchuqa*	Thick bedded to Massive very hard limestone and dolomites
		Balambo and/or Sarmord	Well bedded limestones and marl
Jurassic	Late Middle	Chia Gara, Barsarin,‹ Naokelekan and Sargelu	Mainly bedded to massive dolomites, limestone and marl
	Early	Sehkaniyan, Sarki and Baluti	Mainly limestone, dolomites, thin bedded limestone and shale

Formations marked with a sign (*) are competent, ( ) indicates the possible detachment level

3.1Methodology

3.1. Data

ASTER consists of three different subsystems each system has a spatial resolution and spectral wave length that different from each others: the Visible and Near InfraRed (VNIR) is 15m spatial resolution , the ShortWave InfraRed (SWIR) 30m spatial resolution, and the Thermal InfraRed (TIR) 90m spatial resolution

(Abrams and Hook, 2002). The ASTER level 1A scene was used to extract DEMs with a resolution of 15m. The ASTER data was acquired on 15th September 2006 and the image is free from clouds. In addition, we used eleven QuickBird scenes obtained from the Ministry of Planning (Iraq) and acquired on 28th August 2005. These scenes are orthorectified, and radiometrically corrected with eight-bit dynamic range and 0.6m spatial resolution. QuickBird scenes have three visible spectral bands, blue (0.45 to 0.52 μm), green (0.52 to 0.60 μm) and red (0.63 to 0.69 μm). The three visible spectral bands data were pan-sharpened using the University of New Brunswick (UNB) algorithm (Alparone *et al.*, 2007).

The major maps were used for this research comprises geological and topographical of 1:100,000 scales. QuickBird images were used as a base to georeference all maps. QuickBird images exhibit a perfect corresponding with the ground truth coordinate, which are tested during the field observation using tracking analysis. Seventy field check points having WGS84 datum and UTM projection within zone 38N. Moreover, the geological map was digitalized after (Ibrahim *et al.*, 1984; Sisakian, 1998) and updated depend on geological map reported by (Omar, 2005), field observation and interpretation of QuickBird images.

3.2. Software

ERDAS IMAGINE V.13 software was used to perform the data, e.g. (layer stack and subset). Environment for Visualizing Images (ENVI) V.4.7 software was used for DEMs extraction, ArcGIS V.10.0 software was used to digitize geological map and topographical features, dip and strike extraction, building of structural contour line and layout the results. Eventually, we integrated ArcGIS and Surfer V.11 softwares to produce Digital Surface Model (DSM) of Bekhme Formation in Korek Anticline and display 3D representation of this model. Stereonet V.8.9 was used for projecting linear and planar features such as fold axes and axial planes.

3.3. Method

3.3.1. DEMs Generation from ASTER Stereo Data

Many researchers used DEMs generated from whether satellite stereo data or produced by radar sensor. One of the most common to generate DEMs is stereoscopic images of ASTER data. The ASTER aboard the Terra satellite was designed to generate along-track stereo images and optical stereoscopic DEMs from the VNIR band 3 normal view nadir (3N) and backward view (3B)."ASTER L1A data are formally defined as reconstructed, unprocessed instrument data at full resolution. This product contains depacketized, demultiplexed, and realigned instrument image data with geometric correction coefficients and radiometric calibration coefficients appended but not applied"(Abrams and Hook, 2002). Level 1A data are destriped using the respective parameters provided by the image header (Kaab, 2005). ASTER owns very high geometric accuracy even if any Ground Control Points GCPs is not available (Watanabe, 2006). The high spatial resolution DEMs can be generated from ASTER level 1A data up to 10m relative accuracy without ground control depending on users operating their own software (Abrams and Hook, 2002). The relative elevation values obtained are within 5% of the absolute values and the absolute accuracy for relative elevation values with a base-to-height (B/H) ratio of 0.6 is better then ±20m with a confidence level of 90% (Toutin, 2008).

3.3.1.1. Workflow of DEMs Generation from ASTER Data

The DEM extraction process requires a stereo-pair of images containing rational polynomial coefficients (RPCs) positioning from aerial photography or pushbroom sensors(ENVI, 2009). Since, ASTER level 1A data has the parameters of RPCs appended within metadata information, which are provided the opportunity to apply geometric correction and to orthorectify these data. After we apply building RPCs to extract the exterior orientation in the images, header, the results were used in DEM extraction wizard provided with ENVI software to generate relative DEMs as shown in the workflow (Figure 3). Figure (4) displays the result of the DEMs generated from ASTER band 3N and 3B stereo-pair.

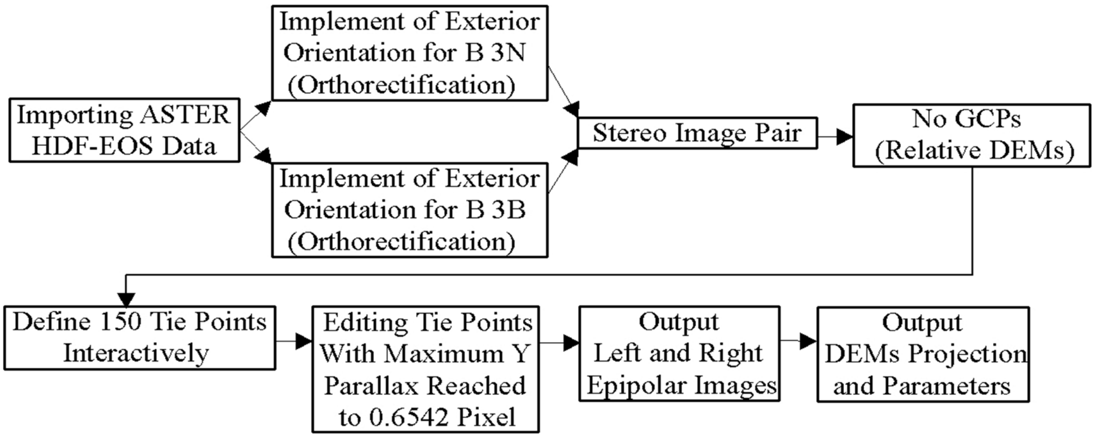

Figure 3. Processing flow of DEMs generation from ASTER band 3N and 3B stereo-pair.

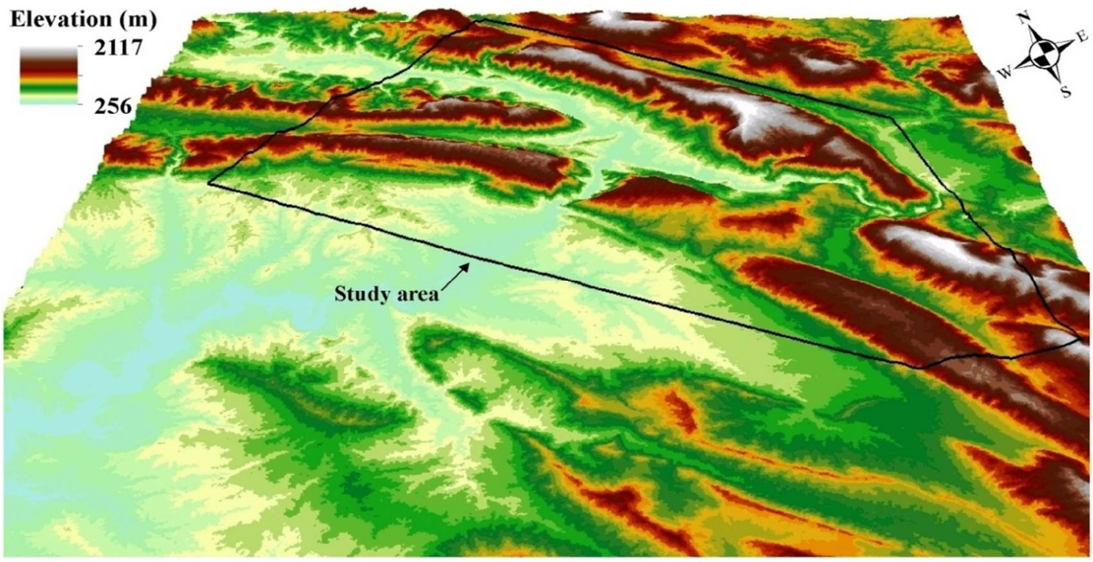

Figure 4. Perspective view of the 3D texture model of the DEMs generated from ASTER band 3N and 3B stereo-pair.

3.3.2. Attitudes Extraction

Building of Structural Contour Lines (SCL) method to extract attitude of strata has a deep root in structural geology. This method was used to extract attitude of the bedding plane not only depending on DEMs, but also by selecting some well exposed rocks with the help of high spatial resolution of QuickBird images. We used the ArcGIS software, which has the ability to create a line feature class of contours (isolines) from a raster surface such as DEMs.

As (Toutin and Cheng, 2001) reported, we derived Topographical Contour Lines (TCL) with contour interval of 30m from DEMs of 15m spatial resolution that is generated via ASTER stereo-pair data, and overlying these TCL with the QuickBird images to discover the intersection between the TCL and the exposed rocks of the bedding plane, particularly in the V-shape valley (downstream dipping valley) or the flat iron phenomenon. However, the intersection points can be used to draw SCL in many locations, where find such as these phenomena. The three or four points occurred on sequentiality TCL can be used for drawing parallel SCL (Figure 5). So the inclination can be calculated by the changing in elevation divided by the distance between two SCL (Equation 1).

$$\text{Tan } \alpha = \Delta Z / D \qquad (1)$$

where α is the dip angle of the bedding plane, ΔZ is the difference in elevation between the 2 TCL and D is the orthogonal distance between the SCL. However, the calculation of dip angle can be used the inverse tangent of the dip as showing below (Equation 2).

$$\alpha = \tan^{-1} \Delta Z / D \qquad (2)$$

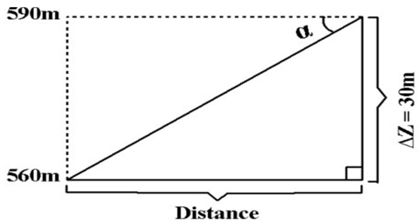

The process of measuring inclination layer depending on SCL requires presence of planar surface of the layer. All the SCL on a surface must be parallel if the surface is planar. Non parallel SCL on a surface indicate that the surface is not planar, such as folded beds. As in some case should be taken into consideration the sensitivity to change in the dip angle and dip direction, where the SCL may be not parallel locally. Predominately, when there is a curviplanar (i.e. curved surfaces) or change of dip direction on both sides of the V-shape valley or the flat iron phenomenon. Therefore, we should rely on three points to draw parallel SCL (Figure 5).

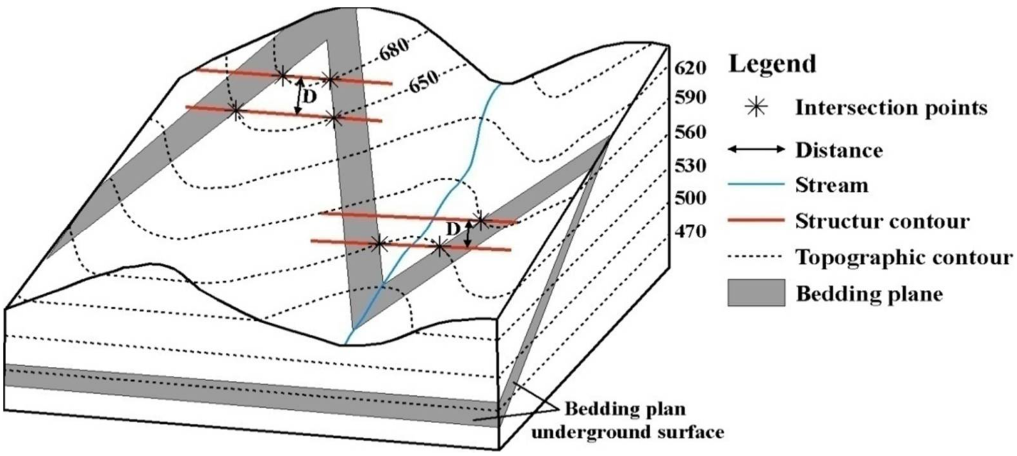

Figure 5.Example of a diagram showing the relationship between TCL and SCL.

3.3.2.1. Result of Attitudes Extraction

ArcGIS software provided the facilities to implement such applications (i.e., building SCL and measuring the spatial orientation). The dip angle was calculated by measuring the orthogonal distance between two successive SCL in the ArcMap environment (Figure 6).Where, the dip angle value obtained from applying the equation (2). The SCL is equal to strike of bedding plane and thus, it represents the trend of the local SCL and can be measured depending on the azimuth of the line in ArcMap environment. The azimuth is expressed in positive degrees from 0º to 359º, measured clockwise from the true north. Also, we measured the dip direction in the same way, which is conventionally normal to strike. We calculated strike, dip direction and dip angle at 85 locations. The results consist of the database, which are accommodated strike, dip direction and dip angle attributes in ArcGIS environment and some of these measurements plotted in Figure (7).

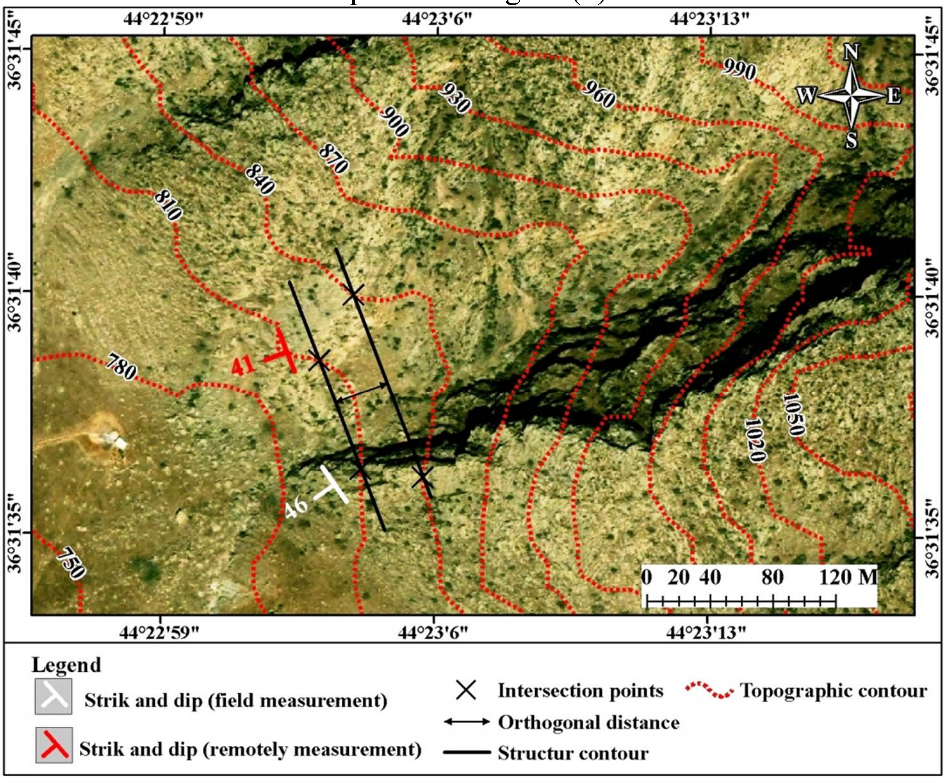

Figure 6. Red: Green: Blue 3:2:1 of QuickBird image overlaying by TCL showing an example of building SCL with dip and strike of the field measurement and remotely extraction in the V-shape downstream dipping valley NW limb of Harir Anticline.

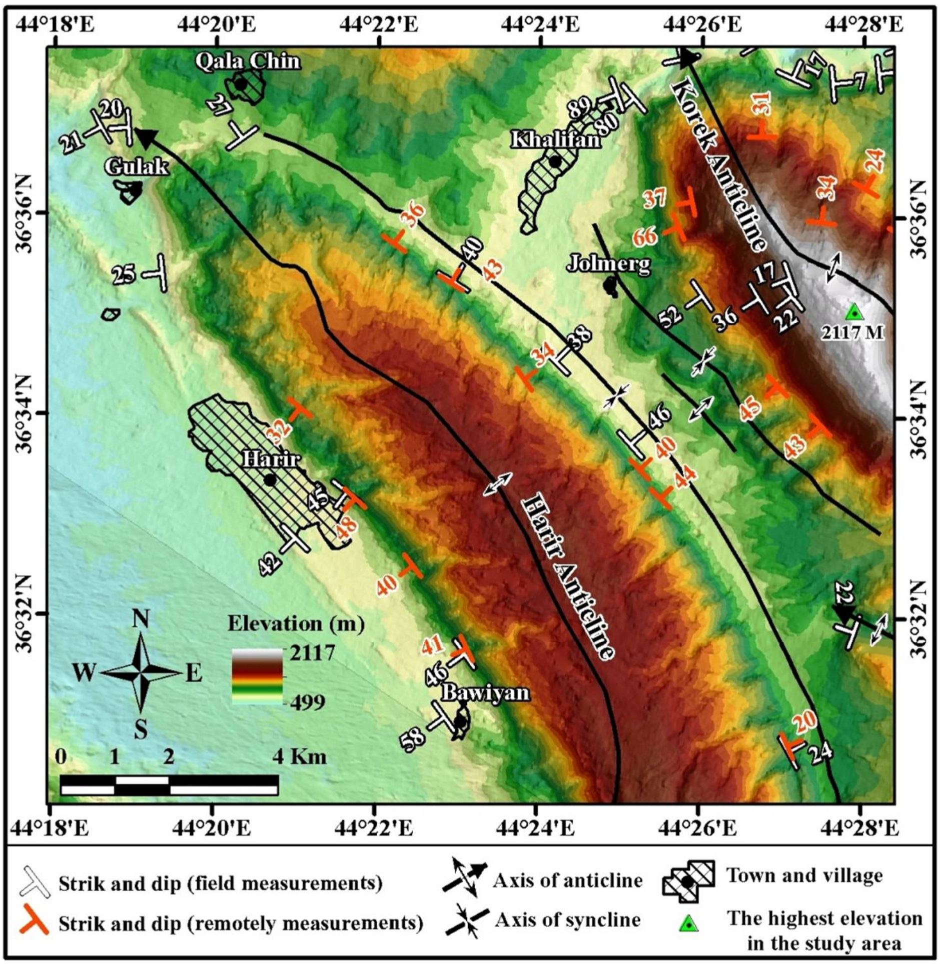

Figure 7. Color coded of (DEMs) generated from ASTER data showing the locations of some attitude measurements by remote sensing data and field investigation of Harir and Korek Anticlines.

Attitudes data in this study were acquired mainly from field investigation and remote sensing products, which are used in geometrical analysis for the major fold classifications within the studied region except Bradost Anticline (Fig. 8 and 9) and (Table 2). According to Omar, (2005), the complexity of Bradost Anticline came from the location in the Imbricated Zone (IZ) between the Zagros suture units and the Zagros Fault Thrust Belt (ZFTB). This fold affected by many thrust and Strike-slip faults, which are observed during field work and from the interpretation of QuickBird images. Also overturning of the strata is noticed locally on the southwestern limb where the beds dips have northeastwards steeply inclination. A geometrical characteristic of Bradost Anticline differs in different sector. It can be divided into three sectors. The middle sector differs from the northwestern and southeastern sectors by increasing in the dip angle of the southwestern limb, which tends to be vertical dipping and overturn where the beds dip steeply northeast wards (Figure 10). While, the southeastern sector decreases in the dip angle of the southwestern limb from other sectors. Although, the extraction of 33 oriented bedding planes using remotely sensed data with 15 stations from the field work, but it is still inadequate to represent the true geometry of this anticline. Thus, the Bradost Anticline did not classify by using graphical method in Stereographic projection.

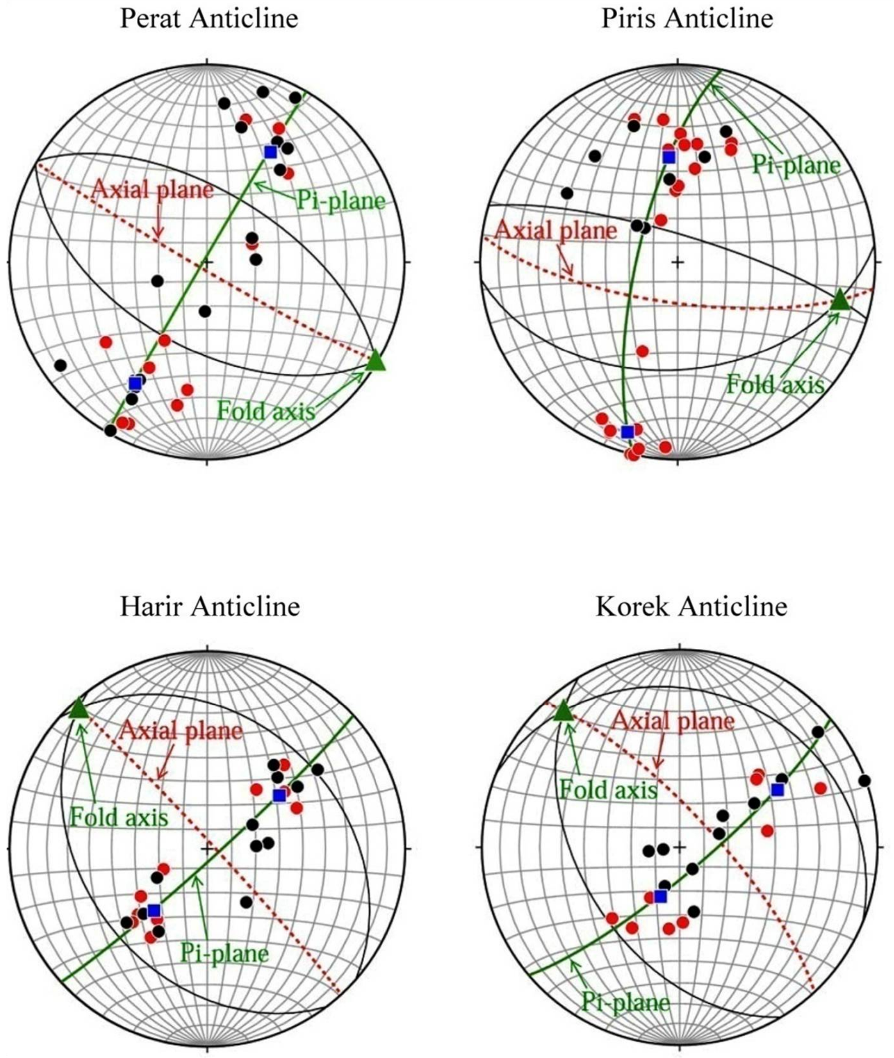

Figure 8. Bedding planes attitude presented in stereographic projections (equal area, lower hemisphere). Black dots indicate field measurements, red dots are remotely measurements, blue squares represent mean poles of bedding planes attitude from remotely and field measurements, and green triangles represent the calculated π pole corresponding to the best fit cylindrical fold axis.

Table 2: Geometrical analysis of the anticlines in the study area

Fold name	Attitudes of axial plane	Interlimb angle	Attitudes of fold axis	Attitudes of mean poles		Attitudes of planes from mean poles	
				NE limb	SW limb	NE limb	SW limb
Perat	210/87	65º	120/01.4	211/29	030/36	031/61	210/54
Piris	188/73	60º	103/17	197/11	355/45	017/79	175/45
Korek	047/76	114º	320/10	202/68	059/42	022/22	239/48
Harir	047/88	110º	318/04	221/56	053/53	041/34	233/37

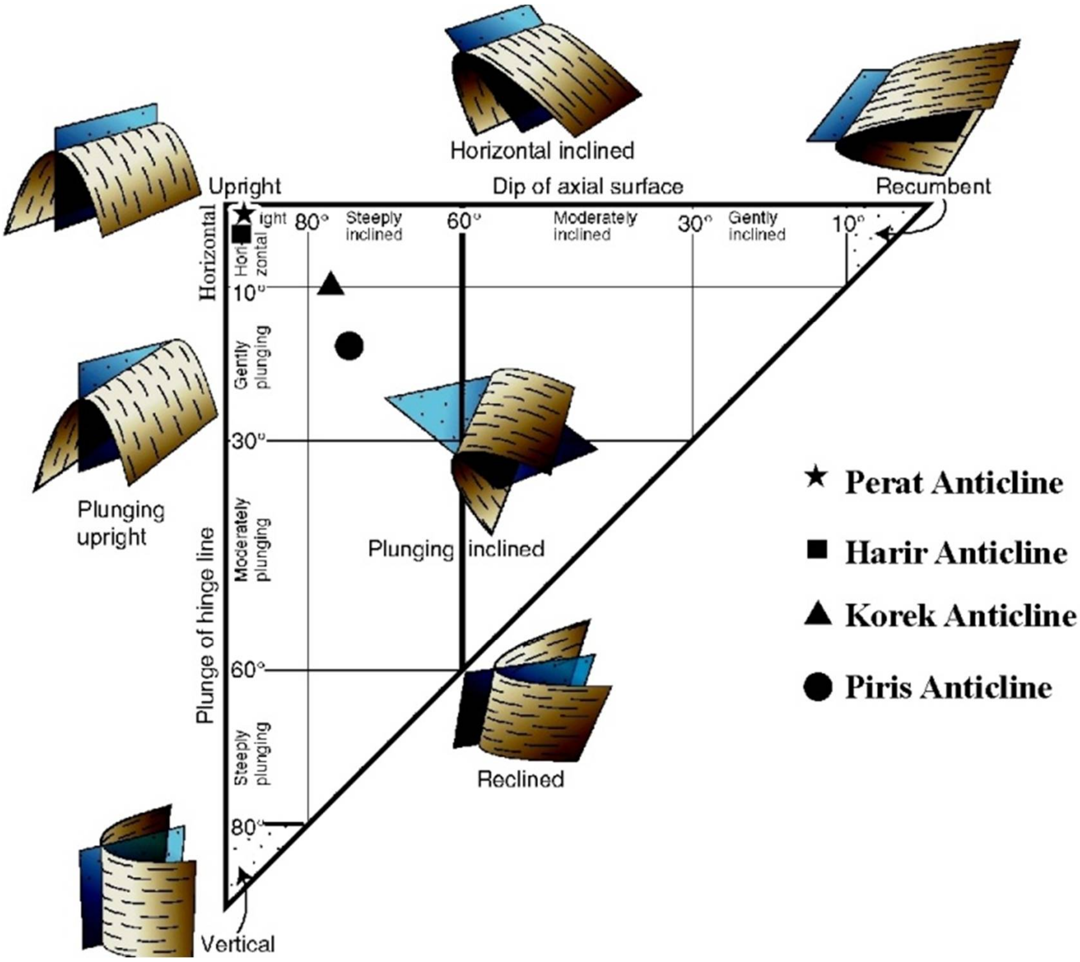

Figure 9. Classification of folds within the study area, according to Fleuty (1964).

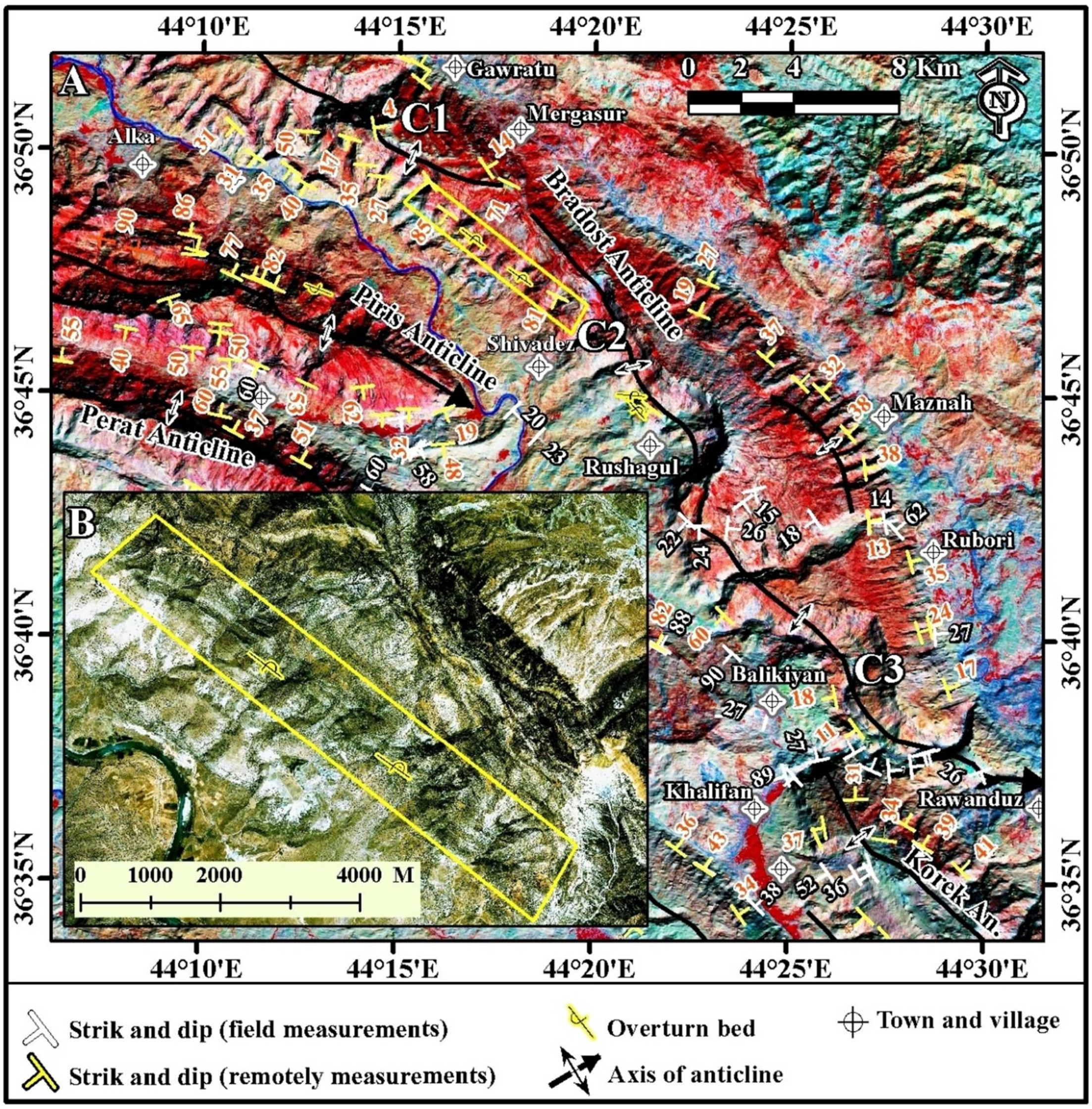

Figure 10. (A) ASTER image R: G: B 3:2:1 showing the three sectors of Bradost Anticline, C1 is the NW sector, C2 is the middle sector, and C3 is the SE sector.(B) QuickBird image RGB 321 showing a part of the southwestern limb of the Bradost Anticline in the middle sector where the beds are overturned.

3.3.2.2. Statistics of Attitudes Remotely Measurements

Attitude measurements of the layers have been collected during the field work based on average measurements for each site. The results of remotely measurements are validated at 10 sites (Figure 11a). We found a good direct linear relation between remotely and field measurements (Figure 11b and c). For the dip angle plot (Figure 11b) the statistical correlations is > 0.98 (the slope is 0.9973 and the intercept is 1.516). While, the dip direction plot (Figure 11c) for the statistical correlations is > 0.99 (the slope is 0.9533 and the intercept is 4.8089). The box and whisker plot (Figure 11d) reveal more than 50% from the error value of dip direction located in the positive values between 2º to 10º, which means the dip direction of the remotely measurements tend to deviate from field measurements ~ +8º. The deviation of the dip direction might result from mismatches between TCL and QuickBird images. However, the error in dip direction value receded between ±10º. While, the error value of dip angle receded between ±5º and more than 50% of the error value in dip angle located between -3º to +4º (Figure 11d). The results are influenced not only by the vertical and horizontal accuracy of the DEMs, but also by the vertical and horizontal mismatches between DEMs and QuickBird images.

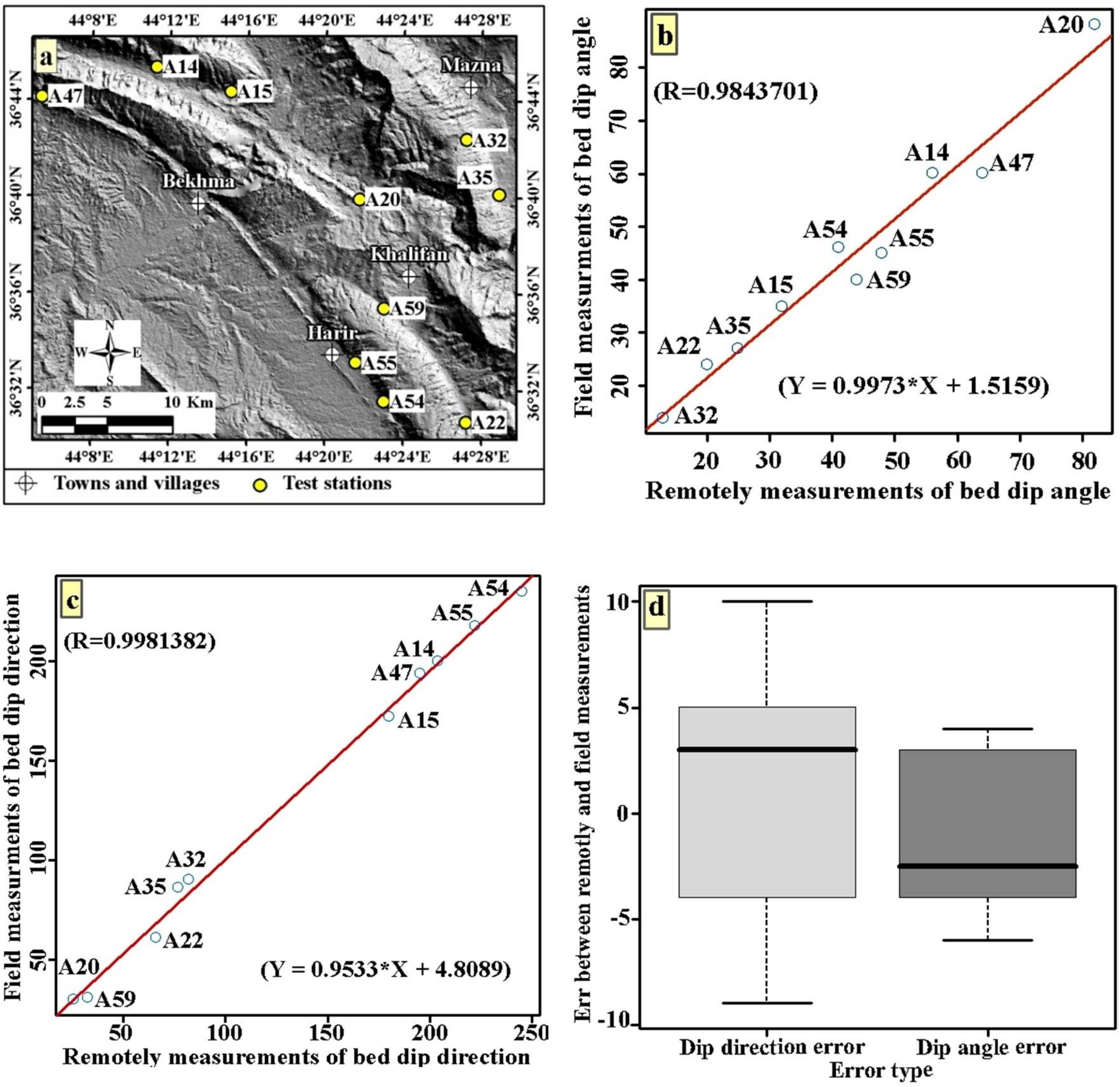

Figure 11. (a) Showing the distribution of the 10 tested stations based on the hillshade derived from DEMs,(b) relation between remotely and field measurements of dip angle, (c) relation between remotely and field measurements of dip direction, and (d) the distribution of error value of the dip direction and dip angle between remotely and field measurements.

3.3.3. Construction of Structure Contours

By definition points on a line of the strike have the same elevations and there being an infinite number of such lines on any inclined plane. When the elevation is known or specified for a particular strike line, then it becomes a structure contour on the plane (Ragan, 2009). We focused to build SCL along the surface of Shiranish and Bekhme Formations. Because they are well exposed and form a good sharp ridge with steeply sloping sides along the eroded flanks of the anticlines. Particularly, were formed around Korek and Harir Anticlines (Figure 12). Each SCL has a value inherit from TCL, which intersect the edges of the bedding plane along the extend surface of the formation. Thus we produce points along the clear exposed surface and each point has the equal elevation.

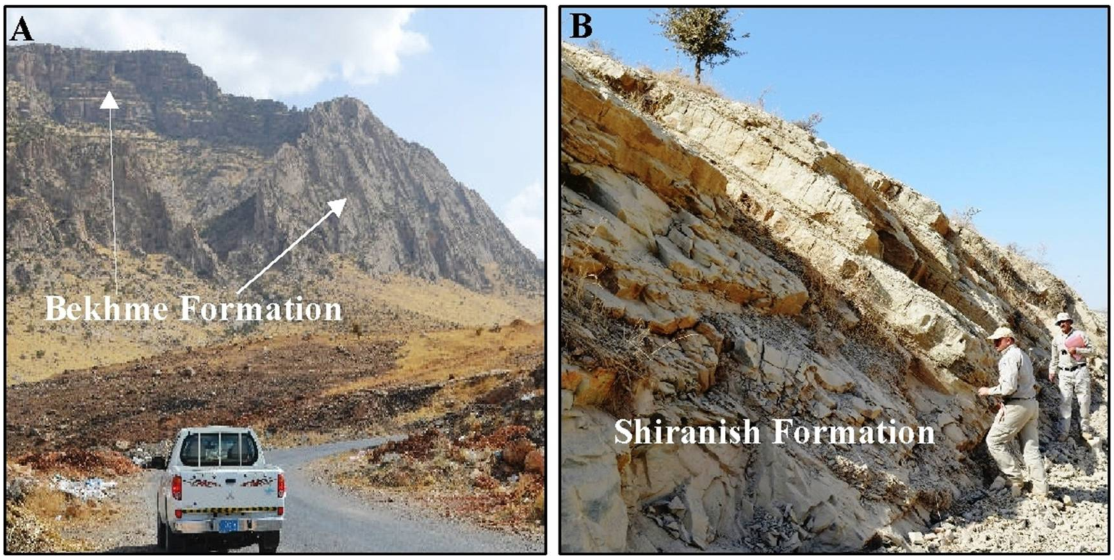

Figure 12. (A) Bekhme Formation in the SW limb of Korek Anticline, photo looking SE direction, (B) Shiranish Formation in the NE limb of Harir Anticline, photo looking NW direction

3.3.3.1. Results of Construction Structural Contours

We constructed structure contours of Bekhme and Shiranish Formations by connecting the points have the same elevation along extend surface. ArcGIS software was used to construct SCL with the help of QuickBird images of high spatial resolution and TCL, which is derived from DEMs of the ASTER data. Figure (13) demonstrated the results, which is revealed that the SCL of the studied area is convex towards the northwest and tend to be E-W in direction. This may be shown the influence of the overlap between Taurus and Zagros trending. Also the SCL explained the geometrical form of the Anticlines within the studied region during the Upper Cretaceous age. The SCL in the northeastern limb of Perat Anticline is closer to the fold axis from the southwestern limb, which exhibits the northeastern limb steeper than the southwestern limb. It means the axial plane dipping to the southwestern direction. While the Bradost Anticline showed quite the opposite. The complexity of Bradost Anticline stood exhibitor to complete building SCL around this anticline. Particularly, in the southwestern limb of the anticline where the formations extremely eroded and affected by many thrust faults. However, we left the more general interpretation and move to more detail description of geometrical properties in Korek Anticline using a technique to build a 3D model.

We used 246 vector points to build raster surface of Bekhme Formation in Korek Anticline. These points were distributed on this surface irregularly. QuickBird images were used to find appropriate geolocation points on this surface. The distribution of points repeated several times to produce a good quality of continuous grid raster data. The values of x, y coordinates of these points inherited from QuickBird images. While, the z value inherited from DEMs of ASTER data. Thus, these points were constructed with x, y, and z, which are local coordinates and attributes using ArcGIS software.

The hinge area in the Korek Anticline is affected by highly fractures and erosional surface and/or entirely thickness of the Bekhme Formation. Particularly, the areas near the fold axis. The z value of the points covered such as these areas different from other points. The difference includes adding the true thickness of the eroded layer to the z value. The true thickness was calculated using the following equation:

$$\text{True Thickness} = D \sin \alpha + \Delta Z \cos \alpha \qquad (3)$$

where α is the dip of the bedding plane, ΔZ is the difference in elevation between the 2 TCL and D is the orthogonal distance between the SCL located in the lower and upper boundaries of the exposed formation.

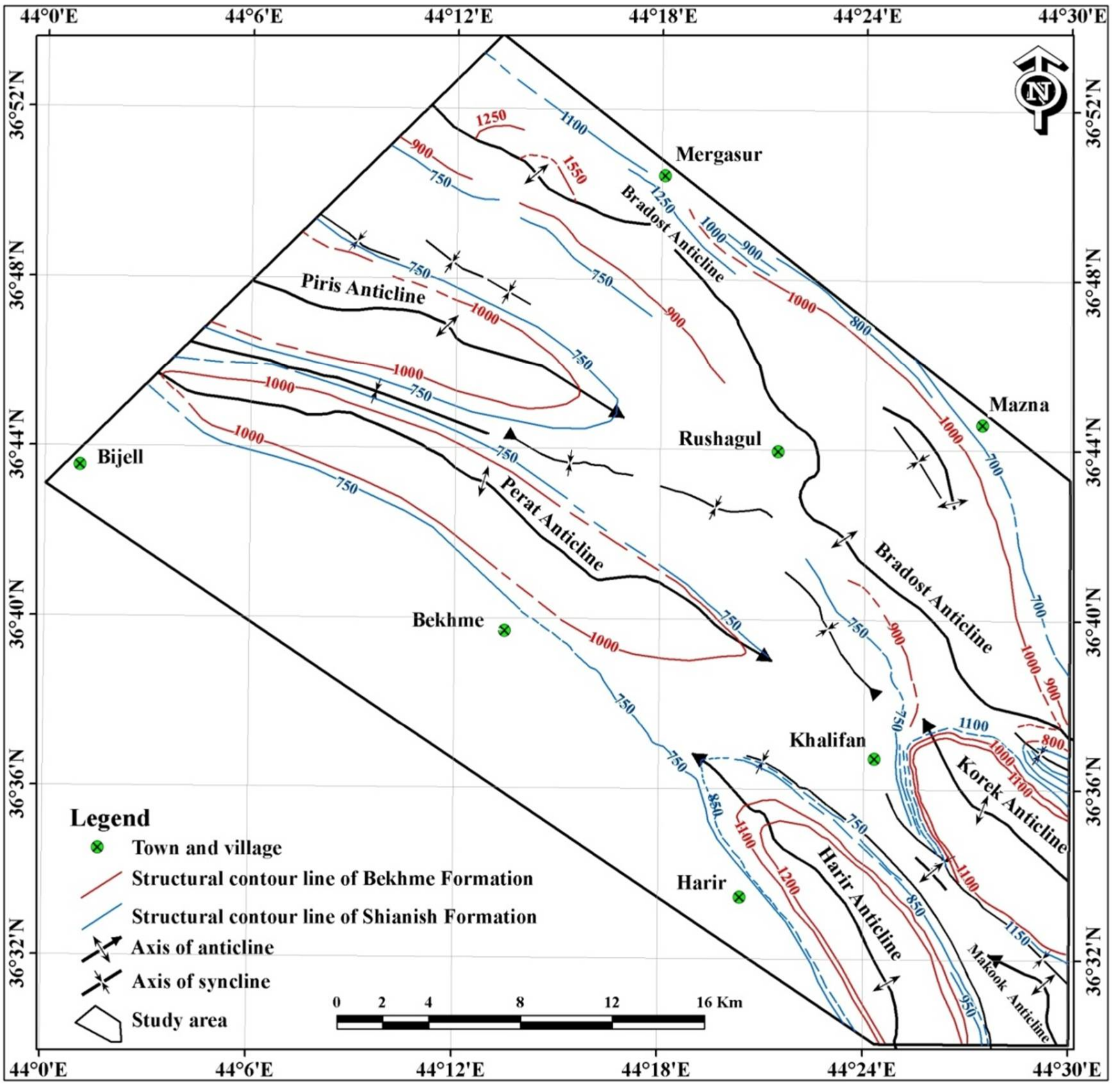

Figure 13: Showing SCL of Bekhme and Shiranish Formations. Discontinuous or dash SCL represents the area where lose the exposed formation or there is no clear intersection between TCL and exposed rocks.

We calculated the eroded thickness at 83 points and the results values were added to the z value or the elevation inherit from DEMs. Subsequently, we interpolated a raster surface from points using a two-dimensional minimum curvature spline technique. The results smooth surface passes exactly through the input points.

The output raster represented the Digital Surface Model (DSM) of Bekhme Formation and exported from ArcGIS software as Grid format. Finally, we used Surfer software to display the raster as 3D model (Figure 14).

The results exhibited the same behavior of geometry in stereographic projections in Figure (8). The southwestern limb is steeper than the northeastern limb, which reflects the inclination of the axial plane toward northeast. There is a convergence between the SCL in the southwestern limb near the plunge area as a result from the thrust fault dipping toward the southwest and the bedding plane tend to be vertical dipping (see Figure 12A). While, in the opposed side of the plunge area within the southwestern limb there are some distortions in the surface of the Model, which are resulted from overturn of the bedding plane where the beds dip northeastwards. The accuracy of this Model increases below SCL with a value of 1500. While, decrease above the same SCL due to the absence of the entire thickness of the formation.

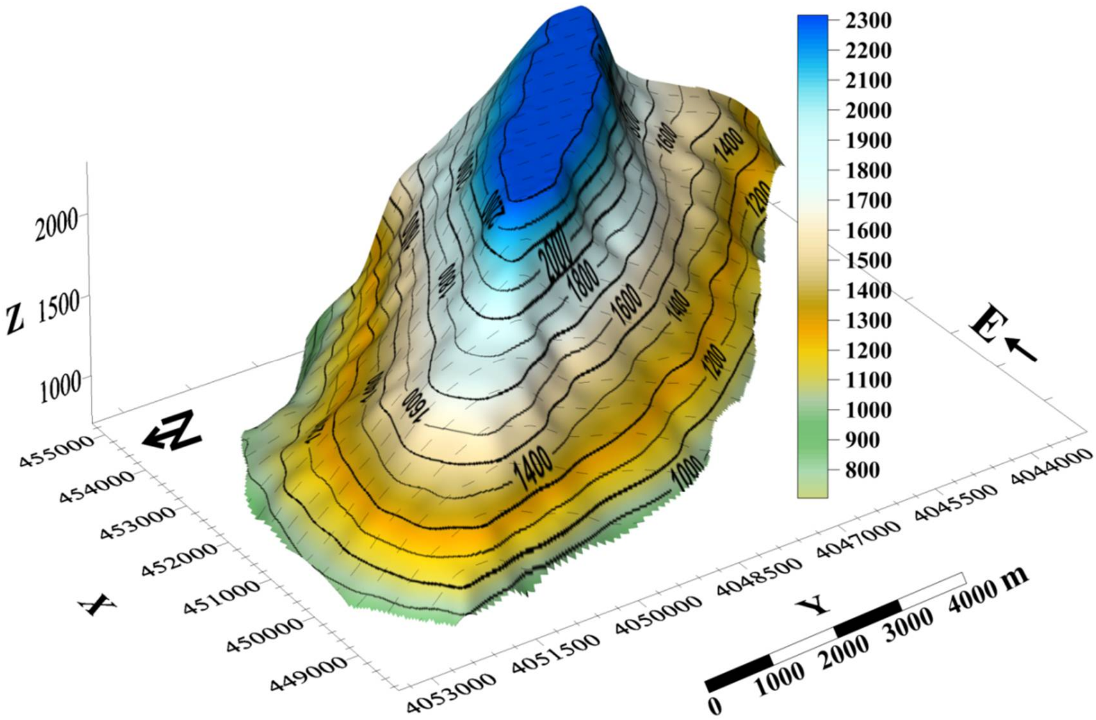

Figure 14: 3D representation of DSM of Bekhme Formation in Korek Anticline.

3.3.4. Geological Map and Structural Elements (Delineating and Updating)

The geological map of Ibrahim *et al.*, (1984) deals with the results of geological interpretation of aerial photographs and Landsat imagery with limited field checking of a considerable part of the northern folded zone of Iraq, which has not been covered by the activities of Geological Survey of Iraq. The geological map at scale 1:100 000 of the Zibar sheet no. (J-38-U/NW) has been compiled based on the data gained from (Hall *et al.*, 1958)and Ibrahim *et al.*, (1984) by Sisakian, (1998). The northeastern corner of this sheet was covered by the geological map produced from field work of (Hall *et al.*, 1958).Our area under investigation located within the Zibar sheet, which is not covered by active geological field works except the southeastern part. Omer, (2005) covered this part by active geological field work with details description of the lithological layer.

However, the previously works that mentioned above with the field work were used to produce and update the geological map of the study area. The maps of the previous works were scanned and georeferenced to the UTM coordinate system in Zone 38 north. These maps were overlying together based on the QuickBird images. We made a comparison between these maps and the differences concentric on the absence of Khurmala Formation in the Tertiary successions except the geological map of Omer, (2005). According to Ibrahim *et al.*, (1984); andSisakian, (1998) the oldest exposed rocks in the core of anticlines are represented by Early Jurassic succession, which are accommodated Sehkaniyan, Sarki and Baluti Formations (Table 1) and (Figure 2). While, the geological map of Omer, (2005) exhibited that the Early Cretaceous represent by upper part of Chia Gara Formation is the oldest Formation exposed in the core of Perat and Bradost Anticlines.

These differences were resolved during the field work with the benefit provided by the high spatial resolution of the QuickBird images. We determined Khurmala/Sinjar Formation during the field work, which consists of dolomitic limestone, crystalline, thick bedded to massive, hard beds and highly fractures (Figure 15C). It forms ridges and cliffs extend along southwestern limbs of Harir and Perat Anticlines and also within Bekhme Syncline (Figure 15A). The thickness increases toward northwest. It is estimated between 50-70m near Bekhme Gorge in the southwestern limb of Perat Anticline (Figure 15A). While, it becomes very thin in the southwestern limb of Harir Anticline.

The oldest exposed formation in the study area belongs to middle Jurassic age. It was estimated according to the thickness of exposed rock under the Cretaceous succession. The thickness of the Jurassic succession was adapted from litterateur review of (Jassim and Goff, 2006; Aqrawi *et al.*, 2010) and the previous field work of (Zebari, 2013), which is not exceeded 400m from the Middle Jurassic to Early Cretaceous ages. The thicknesses of the exposed rocks in the core of anticlines within the study area were measured depending on QuickBird images and DEMs using equation 3. It reveals that the maximum thickness of the oldest exposed rocks under the Cretaceous succession in the core of Piris Anticline is not exceeded 400m. Thus, the exposed rocks in the core of anticlines such as areas in the Bekhme Gorge, Diyana Gorge, east of Shivades village in the Bradost Anticline, core of Korek Anticline, and in the core of Piris Anticline south of Alka village are restricted by Middle Jurassic–Early Cretaceous age (Figure 16).

Moreover, due to the interfingering of the Pila Spi and Gercus Formation (Figure 15B) and the absence of the sharp contact between them, particularly in the northeastern limb of Perat Anticline and within the limbs of Bekhme Syncline. Therefore, those formations are grouped together (Figure 16). The boundaries of all formations were adjusted based on full-scale or zoom of spatial resolution in QuickBird images, which is reached to 1:2000 on scale.

Image interpretation and the field work are emphasized in this work to produce the geological map with some structural elements (Figure 16). Images are used to locate areas where rocks are exposed at the surface and to trace key geologic units across the landscape, and make important distinctions between landforms, relate them to the geologic processes that formed them, and thus interpret the geologic history of the area (Lillesand *et al.*, 2004). Also the geological map can be portrayed and identification of landforms, rock types, and rock structures (folds, faults, fractures) and structures on a map or other display in their correct spatial relationship with one another (Lillesand *et al.*, 2004).

We delineated the trace of the thrust fault and the contact between Stratigraphic units depending on images interpretation of the QuickBird images, stereo-pair and color composite of ASTER image. As well as, the field investigation with the previous field works of Omar, (2005); Al-Jumaily *et al.*, (2012); Csontos *et al.*, (2012); Zebari, (2013) were depicted the structural model of the study area. Csontos *et al.*, (2012) and Zebari, (2013) highlight interpreted of the seismic sections within the study area. These interpretations exhibit that the thrust and back-thrust in addition to strike-slip faults system play a key role in structural forms in the study area. The thrust system depicted the form of anticlines between a thrust and its conjugate back-thrust forms a pop-up and triangle zone model. However these interpretations deal with the trace of the thrust faults were delineated based on available satellite images, which are covered the study area. The result is illustrated in Figure (16).

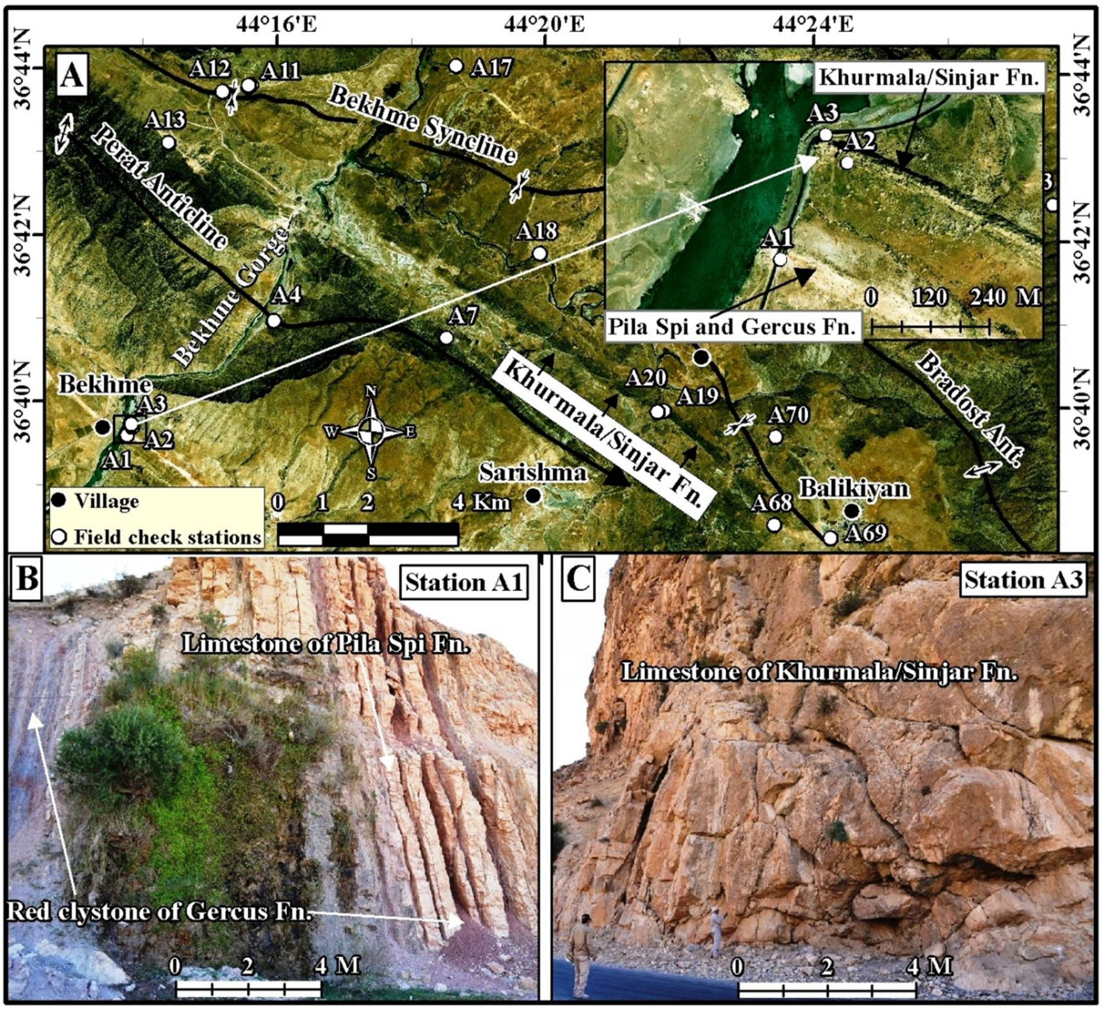

Figure 15. (A) QuickBird imagery R3:G2:B1 showing the distribution stations of the field work and the ridges of Khurmala/Sinjar, Pila Spi and Gercus Formations.(B) and (C) Field photo in the southwestern limb of Perat Anticline near Bekhme gorge (station A1) looking SE direction showing the interfingering between Pila Spi and Gercus Formations, (station A3) looking SSE direction showing Khurmala/Sinjar Formation.

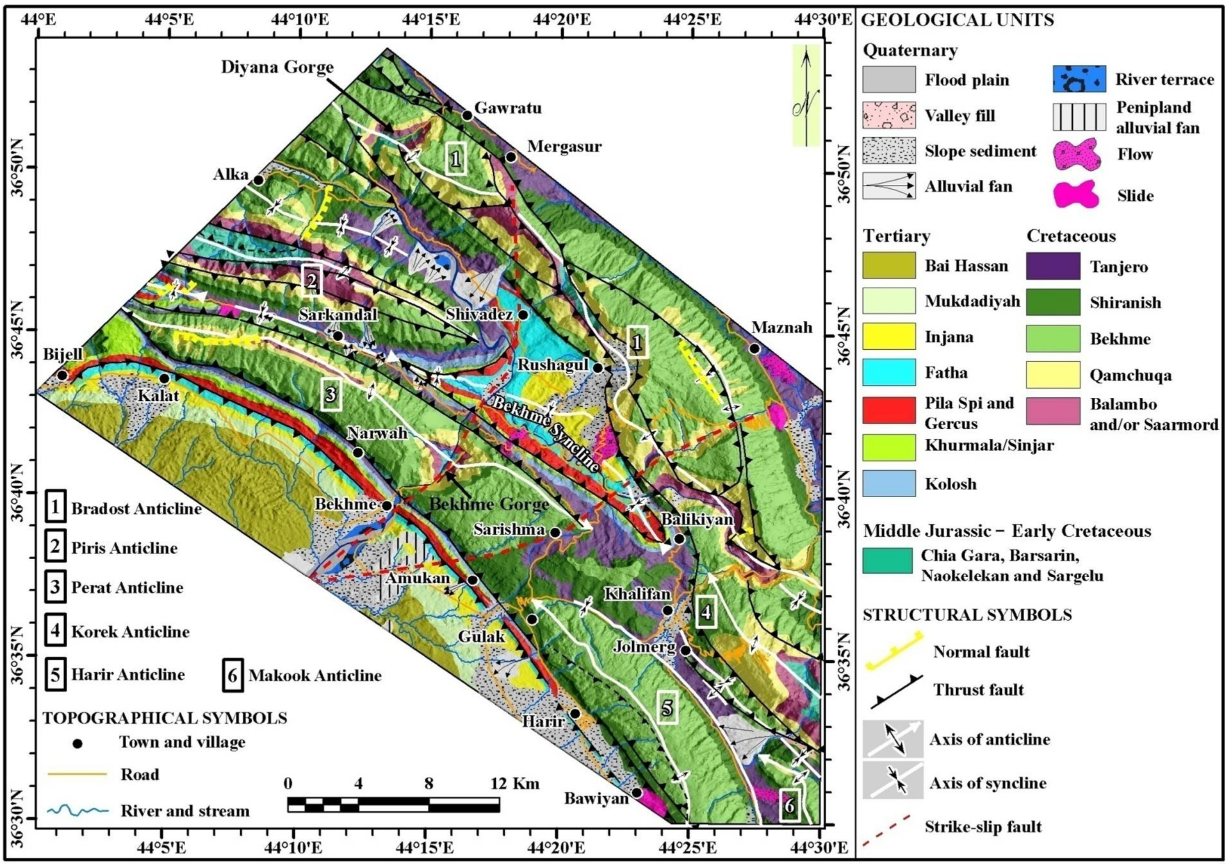

Figure 16. Geological and structural map of the study area.

Conclusion

The style of deformation in the overlying Cenozoic units is complex and appears to be controlled by changing mechanical stratigraphy across the Zagros fold thrust belt. In this area pre-existing incompetent beds play an important role in the localization and geometry of folds. The maps (Figure2 and 16) also depict major reverse and thrust faults. The majority of folds visible on the satellite image in Figures (1 and 4), display east-west in it's the NW part and then deflection in trend to a NE-SW orientation in its SE part.

As discussed, the complex structure of the NE part of Iraq was generated by persistent shortening toward northeasterly when folds and thrusts at all structural levels were in very close association, and developed simultaneously. Due to continuous squeezing, the study area becomes tighter whilst increasing thrusting occurred on the decollement surfaces of marl or gypsum of Triassic succession or Fatha Formation. These thrusts are envisaged as thrusts which splay to the northeast and to the southwest. We suggest that the same faults could be possibly regarded as back-thrusts. This model agrees with pop-up and triangle zone model and this model explains why the study area was affected by a continuous fold thrust sequence of tectonic deformation. This model involves a squeezing of the upper sediments, which are located above the detachment thrust against the Lower Triassic succession. The different orientations of the various folds and thrusts could be related to the shape of the Alpine thrust region.

Acknowledgments

We would like to express our great thanks to Arsalan Ahmed Othman in TU Berakademie Freiberg, for providing some references and advices. In addition, the authors want to sincerely thank Prof. Dr. Mazin Y. Tamar-Agha in Department of Geology, University of Baghdad for assisting in the completion to update geological map. Finally, we are grateful to the Geological Survey of Iraq and Ministry of Planning in Iraq for providing the data and supporting the fieldwork.

References

Abrams, M., and Hook, S., 2002. ASTER user handbook (Version 2): Jet Propulsion Laboratory/EROS Data Center, USA, 135 p.

Al-Jumaily, I. S., Adeeb, H. G. M., Al-Hamdani, R. K., and Dawlat, M. S., 2012. Structural Analysis and Tectonic Interpretation of Brittle Failure Structures at Perat Anticline – NE Iraq. Iraqi National Journal of Earth Sciences, v. 12, p. 17-42.

Al-Kadhimi, J. A. M., Sissakian, V. K., Fattah, A. S., and Deikran, D. B., 1996. Tectonic Map of Iraq, scale 1:1000000, 2nd edit. GEOSURV, Baghdad, Iraq, p. 1-38.

Alavi, M., 1994. Tectonics of the Zagros erogenic belt of Iran: new data and interpretationsTectonophysics, v. 229 p. 211-238.

Allison, D. T., 2004. Structural Geology Laboratory Manual, 3nd edit, University of South Alabama.

Alparone, L., Wald, L., Chanussot, J., Thomas, C., Gamba, P., and Bruce, L. M., 2007. Comparison ofpansharpening algorithms: Outcome of the 2006 GRS-S data-fusion contest. IEEE Transactions on Geoscience and Remote Sensing, v. 45, p. 3012–3021.

Aqrawi, A. M., Goff, J. C., Horbury, A. D., and Sadooni, F. N., 2010. the Petroleum Geology of Iraq: UK, Scientific Press Ltd.

Bennison, G. M., 1990. An Introduction to Geological Structures and Maps, Arnold, 66 p.

Büyüksalih, G., Kocak, M. G., Oruc, M., Akcin, H., and Jacobsen, K., 2003, DEM GENERATION BY ASTER AND TK350: Joint Workshop "High Resolution Mapping from Space 2003".

Csontos, L., Sasvári, Á., Pocsai, T., Kósa, L., Salae, T. M., and Ali, A., 2012. Structural evolution of the northwestern Zagros, Kurdistan Region, Iraq: Implications on oil migration. GeoArabia, v. 17, p. 81-116.

Cuartero, A., Felicísimo, A. M., and Ariza, F. J., 2012, Accuracy of Dem Genaration From Terra-Aster Stereo Data: International Society for Photogrammetry and Remote Sensing ISPRS Archives, p. 4.

Dadon, A., Peeters, A., Ben-Dor, E., and Karnieli, A., 2011. A Semi-automated GIS Model for Extracting Geological Structural Information from a Spaceborne Thematic Image. GIScience & Remote Sensing, v. 48, p. 264–279.

Eckert, S., Kellenberger, T., and Itten, K., 2005. Accuracy Assessment of Automatically Derived Digital Elevation Models from ASTER Data in Mountainous Terrain. International Journal of Remote Sensing, v. 26, p. 1943–1957.

ENVI, 2009. DEM Extraction Module User's Guide v. 4.7, ITT Visual Information Solutions.

Fleuty, M. J., 1964. The description of folds. Proceedings of the Geologists' Association, v. 75, p. 461-492.

Fossen, H., 2010. Structural Geology: United States of America, Cambridge University Press, 457 p.

Hall, P. K., 1958., The Geology of Rlkan and Zibar, In., Bolton, C. M. G., Cobbett, G. P. R., Hall, P. K., Stevenson, P. C., and Villiers, P. R. D., 1958. Report for Summer Season: 1957. GEOSURV, Int. Rep. No. 270, Baghdad, Iraq, p. 6-35.

Hasbargen, L. E., 2012. A test of the three-point vector method to determine strike and dip utilizing digital aerial imagery and topography. Geological Society of America Special Paper, v. 492, p. 199-208.

Hirano, A., Welch, R., and Lang, H., 2003. Mapping from ASTER stereo image data: DEM validation and accuracy assessment. ISPRS Journal of Photogrammetry and Remote Sensing, v. 57, p. 356-370.

Ibrahim, S. B., Ahmed, F. T., Jawad, S. A., Kocho, K. I., and Al-Azzawi, A. R., 1984. Report on The Photogeology of a Part of The Folded Zone-Northern Iraq. GEOSURV, Int. Rep. No. 1376, Baghdad, Iraq.

Jassim, S. Z., and Goff, J. C., 2006. Geology of Iraq, Published by Dolin, Pragh and Moravian Mueseum, Brno, 302 p.

Kääb, A., 2005. Remote Sensing of Mounain Glaciers andPermafost Creep, Geographisches Institut der Universität Zürich, 231 p.

Kääb, A., Huggel, C., Paul, F., Wessels, R., Raup, B., Kieffer, H., and Kargel, J., 2002, Glacier Monitoring from ASTER Imagery: Accuracy And Applications: E ARSeL-LISSIG-Workshop Observing our C ryosphere from Space, p. 43-53.

Lang, H. R., Welch, R., Miyazaki, Y., Bailey, G. B., and Kelly, G., 1996. ASTER along-track stereo experiment: a potential source of global DEM data in the late 1990s, Infrared Spaceborne Remote Sensing Denver, Marija S. Scholl; Bjorn F. Andresen.

Lillesand, T. M., Kiefer, R. W., and Chipman, J. W., 2004. Remote Sensing and Image Interpretation: Hoboken, NJ, USA, John Wiley & Sons, Inc.

Oliveira, C. G., and Paradella, W. R., 2008. An Assessment of the Altimetric Information Derived from Spaceborne SAR (RADARSAT-1, SRTM3) and Optical (ASTER) Data for Cartographic Application in the Amazon Region. sensors, v. 8, p. 3819-3829.

Omar, A. A., 2005. An Integrated Structural and Tectonic Study of the BinaBawi-Safin-Bradost Region In Iraqi Kurdistan: Ph.D. thesis, University of Salahaddin, Unpub, 286 p.

Poli, D., Dolci, C., and Remondino, F., 2005, Dtm Extraction from Middle-Resolution Satellite Imagery for Landscape Modeling and GIS Applications: 6a Setmana Geomatica.

Ragan, D. M., 2009. Structural Geology An Introduction to Geometrical Techniques: United States of America, New York, Cambridge University Press.

Reif, D., Grasemann, B., and Faber, R. H., 2011. Quantitative structural analysis using remote sensing data: Kurdistan, northeast Iraq. Journal of the American Association of Petroleum Geologists AAPG Bulletin, v. 95, p. 941-956.

Sisakian, V. K., 1998. The geology of Erbile and Mahabad quadrangle sheet NJ-38-15, Scale 1:250000. GEOSURV, Int. Rep. No. 2462, Baghdad, Iraq.

Sissakian, V. K., 2012. Geological Evolution of the Iraqi Mesopotamia Foredeep, Inner Platform and Near Surroundings of the Arabian Plate. Journal of Asian Earth Sciences, v. 72, p. 152-163.

Toutin, T., 2008. ASTER DEMs for Geomatic and Geoscientific Applications: a Review. International Journal of Remote Sensing, v. 29, p. 1855–1875.

Toutin, T., and Cheng, P., 2001. DEM generation with ASTER stereo data. Earth Observation Magazine, v. 10, p. 10-13.

Watanabe, H., 2006. Accuracy of Aster Geolocation and DEM and Their Application International Society for Photogrammetry and Remote Sensing ISPRS Archives. The Netherlands, p. 4.

WVDEP, 2005. Geologic Handbook, West Virginia Department of Environmental Protection, 118 p.

Zebari, M., 2013. Geometry and Evolution of Fold Structures Within the High Folded Zone: Zagros Fold-Thrust Belt, Kurdistan Region-Iraq, University of Nebraska-Lincoln, DigitalCommons@ University of Nebraska-Lincoln, 91 p.

Zhao, S., Cheng, W., Zhou, C., Chen, X., Zhang, S., Zhou, Z., Liu, H., and Chai, H., 2011. Accuracy assessment of the ASTER GDEM and SRTM3 DEM: an example in the Loess Plateau and North China Plain of China. International Journal of Remote Sensing, v. 32, p. 8081–8093.